Enhanced sampling in numerical path integration: An approximation for the quantum statistical density matrix based on the nonextensive thermostatistics

T. W. Whitfield and J. E. Straub
Department of Chemistry, Boston University, Boston, Massachusetts 02215
(Received 10 July 2001; published 20 November 2001)

Here we examine a proposed approximation for the quantum statistical density matrix motivated by the nonextensive thermostatistics of Tsallis and co-workers. The approximation involves replacing the physical potential energy with an effective one, corresponding to a generalized nonextensive statistical ensemble. We examine the convergence properties of averages calculated using the effective potential, and introduce a related method for enhanced sampling in numerical path integration. As a necessary measure, path integral energy estimators are introduced for potentials that involve explicit temperature dependence. This sampling method is found to be effective for path integral simulations involving broken ergodicity.

DOI: 10.1103/PhysRevE.64.066115 PACS number(s): 05.10.−a, 05.30.−d

I. INTRODUCTION

Path integration is a widely employed means of calculating quantum mechanical averages for thermodynamic observables. Much of the utility of this technique in computer simulation is related to the well known isomorphism [1,2] between the path integral expression for the partition function of a single quantum particle and that of a classical polymer ring having N pseudoparticle ''beads.'' Due to this isomorphism, many of the techniques from classical simulations may be applied to quantum problems. Difficulties arise however, when the number of beads N, required to accurately represent the quantum system, becomes large [3], and/or when barriers separating potential minima are high. Both of these situations occur at low temperatures. In the former case, the bonds between the beads in the isomorphous polymer chain become stiff, and long simulation times are required for conformational sampling. In the case of high barriers, tunneling is restricted and the system may manifest a ''broken ergodicity'' [4–6].

To mitigate the problem of stiff bonds in the polymer chain, a number of strategies have been developed. Some of these methods enhance the sampling of the N-bead configurations. These include normal mode techniques for the intrachain interactions [7], which are closely related [8] to Fourier path integral methods [9–11], and the staging algorithm [12]. Other methods move beyond the so-called primitive high-temperature approximation to the discretized action, thereby reducing the required number of beads. Among these techniques are higher-order factorizations of the thermal density operator [13–15], use of the Wigner-Kirkwood expansion [16], generating an effective potential with renormalization group techniques [17], and schemes that make use of exact harmonic propagators [18–22]. Some methods that enhance sampling of classical systems with high barriers have been successfully applied to path integral simulations [7].

In this paper we will explore a formal connection, recently pointed out by Straub and Andricioaei [23,24], between the path integral formulation of quantum statistical mechanics and the nonextensive thermostatistics proposed by Tsallis [25]. This connection, which will be described in a greater detail in the following section, amounts to replacing the physical potential appearing in the propagator with an effective one. Focusing on a pair of simple one-dimensional systems, we compare the convergence properties with those of the standard primitive high-temperature approximation to the propagator, and develop a Monte Carlo method for enhanced sampling in quantum systems with broken ergodicity.

The paper is organized as follows: In Sec. II, we review the connection between path integration and the nonextensive thermostatistics of Tsallis and co-workers. In Sec. III, we derive energy estimators required for application of our effective potential. Section IV outlines the two main computational methods we have used. Section V presents results for a one-dimensional harmonic oscillator and a one-dimensional bistable potential, and Sec. VI concludes the paper.

II. CONNECTION WITH NONEXTENSIVE THERMOSTATISTICS

In one dimension, the primitive path integral expression for the partition function may be constructed beginning with the identity

$$Z=\int dx\rho(x,x;\beta)=\int dx_1\cdots dx_N\prod_{i=1}^{N}\langle x_i|e^{-\beta H/N}|x_{i+1}\rangle, \tag{2.1}$$

where $x_1=x_{N+1}=x$, $\beta=1/kT$ and $\rho(x,x;\beta)$ is the diagonal part of the density matrix. To make this formal expression useful, the density operator is factored using the Trotter product formula [26,27]

$$e^{-\beta(T+V)/N}=e^{-\beta T/N}e^{-\beta V/N}+O(\beta^2/N^2). \tag{2.2}$$

Based upon a relationship between the *classical* density function and the Tsallis statistical distribution function, Straub and Andricioaei [23,24] have suggested the following alternative:

$$e^{-\beta(T+V)/N} \approx e^{-\beta T/N}\left(\frac{1}{1+\frac{\beta V}{N}}\right) = e^{-\beta T/N} e^{-\beta \bar{V}/N}, \tag{2.3}$$

where

$$\bar{V} = \frac{N}{\beta}\ln\left(1+\frac{\beta}{N}V\right) = \frac{1}{\beta(q-1)}\ln[1-(1-q)\beta V], \tag{2.4}$$

and $q = 1+1/N$. Equation (2.4) defines the nonextensive effective potential we will use throughout this paper. $\bar{V}$ has the obvious and important property that $\lim_{(\beta/N)\to 0}\bar{V} = V$; in the high temperature limit, Eq. (2.3) will become equivalent with Eq. (2.2).

Classically, Eq. (2.3) is the so-called Maxwell-Tsallis statistical distribution [28,23,24], a product of the Tsallis distribution over configurations and the Boltzmann distribution over momenta. The effective potential characterizes the classical configurational distribution

$$p_q(x) = \frac{e^{-\beta\bar{V}(x)}}{Z_q} = \frac{1}{Z_q}[1-(1-q)\beta V(x)]^{1/(1-q)}, \tag{2.5}$$

where

$$Z_q = \int dx(1-(1-q)\beta V(x))^{1/(1-q)} \tag{2.6}$$

is the generalized partition function. This distribution is obtained as a result of extremizing the ''generalized entropy'' [25],

$$S_q = \frac{k}{q-1}\int dx p_q(x)\{1-[p_q(x)]^{q-1}\}, \tag{2.7}$$

subject to the constraints,

$$\int dx p_q(x) = 1, \quad \int dx[p_q(x)]^q V(x) = V_q. \tag{2.8}$$

In the limit that $q\to 1$ $(N\to\infty)$, the Boltzmann distribution is recovered. For $q\neq 1$ however, although many of the properties of the Gibbs-Boltzmann statistical mechanics are preserved, thermodynamic state functions like the entropy and internal energy are no longer extensive functions of the system. Note that the second constraint in Eq. (2.8) is one of the several forms that have been explored within the context of the nonextensive thermostatistics [29,30].

Of particular relevance to this work is the transformation of the Tsallis distribution for q different from unity. When $q<1$ (not possible when $q=1+1/N$), the configurational distribution becomes localized around minima on the physical potential, and presents a cutoff for high energies [29,31]. While this may be advantageous for *local* sampling of the configuration space, we do not expect $q>1$ to mitigate the issue of *globally* enhancing the sampling [32]. In contrast, for $q>1$ the distribution becomes broader, and manifests greater probability in barrier regions of the potential energy function. This property has been used to advantage in simulations of classical systems with problems of broken ergodicity [33,34].

Throughout the rest of this work, we employ a symmetric factorization of the density operator

$$e^{-\beta(T+V)/N} = e^{-\beta V/2N} e^{-\beta T/N} e^{-\beta V/2N} + O(\beta^3/N^3). \tag{2.9}$$

In terms of calculating averages for observables that commute with $V(x)$, Eq. (2.9), although a better high-temperature approximation, gives no advantage over equation (2.2), due to the cyclic invariance of the trace. It does, however, preserve the Hermitian property of the density operator, and will be advantageous when directly calculating the average kinetic energy.

For a particle of mass m, substitution of Eq. (2.9) into Eq. (2.1) gives

$$Z = \int dx_1 \cdots dx_N \prod_{i=1}^{N} \rho^{(0)}(x_i, x_{i+1}; \beta/N), \tag{2.10}$$

$$= \left(\frac{mN}{2\beta\hbar^2}\right)^{N/2} \int dx_1 \cdots dx_N \exp[-\Phi(x_1, \ldots, x_N)], \tag{2.11}$$

where

$$\Phi(x_1, \ldots, x_N) = \sum_{i=1}^{N}\left\{\frac{mN}{2\beta\hbar^2}(x_i - x_{i+1})^2 + \frac{\beta}{2N}[V(x_i) + V(x_{i+1})]\right\} \tag{2.12}$$

is the action, and

$$\rho^{(0)}(x_i, x_{i+1}; \beta/N) = e^{-\beta V(x_i)/2N}\rho_0(x_i, x_{i+1}; \beta/N) \times \exp[-\beta V(x_{i+1})/2N]. \tag{2.13}$$

The free particle propagator is

$$\rho_0(x_i, x_{i+1}; \beta/N) \equiv \langle x_i | e^{-\beta T/N} | x_{i+1}\rangle = \sqrt{\frac{mN}{2\beta\hbar^2}}\exp[-mN(x_i - x_{i+1})^2/2\beta\hbar^2]. \tag{2.14}$$

We use the primitive action [Eq. (2.12)] and its effective potential counterpart

$$\overline{\Phi}(x_1,\ldots,x_N)=\sum_{i=1}^{N}\left\{\frac{mN}{2\beta\hbar^2}(x_i-x_{i+1})^2+\frac{\beta}{2N}[\overline{V}(x_i)+\overline{V}(x_{i+1})]\right\} \tag{2.15}$$

throughout this paper.

III. ENERGY ESTIMATORS

Using any method for evaluating path integrals, estimating the energy requires special attention, since the Hamiltonian is not diagonal in the position representation [2,11]. Because our effective potential [Eq. (2.4)] depends explicitly on temperature, we will need to generalize the standard estimators.

A. Thermodynamic estimator

One common energy estimator for path integrals is derived by using the thermodynamic expression for the internal energy

$$E_t=-\frac{\partial}{\partial\beta}\ln Z=\frac{-1}{Z}\frac{\partial}{\partial\beta}Z. \tag{3.1}$$

Taking the β derivative inside the integral in our expression for the partition function [Eq. (2.11)], we arrive at

$$E_t=\left\langle\frac{N}{2\beta}-\frac{Nm}{2\hbar^2\beta^2}\sum_{i=1}^{N}(x_i-x_{i+1})^2+\frac{1}{N}\sum_{i=1}^{N}\left[\overline{V}(x_i,\beta/N)+\beta\frac{\partial}{\partial\beta}\overline{V}(x_i,\beta/N)\right]\right\rangle. \tag{3.2}$$

The terms inside the average constitute the thermodynamic estimator for systems with temperature-dependent potentials. The last term in this estimator vanishes for temperature-independent potentials, giving the standard thermodynamic estimator [2]. With the Tsallis effective potential, we have

$$E_t=\left\langle\frac{N}{2\beta}-\frac{Nm}{2\hbar^2\beta^2}\sum_{i=0}^{N-1}(x_i-x_{i+1})^2+\frac{1}{N}\sum_{i=1}^{N}\left[\frac{V(x_i)}{\left\{1+\frac{\beta}{N}V(x_i)\right\}}\right]\right\rangle. \tag{3.3}$$

We confirm that for β/N small, equation (3.3) goes to the standard estimator.

B. Virial estimator

As an alternative to the thermodynamic estimator, Herman, Bruskin, and Berne [35] developed an estimator based on the quantum virial theorem (see Appendix A for details). This estimator may have better statistical properties than its thermodynamic counterpart [35,36], as N is increased. For temperature-dependent potentials, the virial estimator is

$$E_v=\left\langle\frac{1}{N}\sum_{i=1}^{N}\left[\overline{V}(x_i,\beta/N)+\beta\frac{\partial}{\partial\beta}\overline{V}(x_i,\beta/N)+\frac{1}{2}x_i\frac{\partial\overline{V}(x_i,\beta/N)}{\partial x_i}\right]\right\rangle. \tag{3.4}$$

For the Tsallis effective potential, Eq. (3.4) becomes

$$E_v=\left\langle\frac{1}{N}\sum_{i=1}^{N}\left[\frac{V(x_i)+\frac{1}{2}x_i\frac{\partial V(x_i)}{\partial x_i}}{\left\{1+\frac{\beta}{N}V(x_i)\right\}}\right]\right\rangle. \tag{3.5}$$

By construction, the averages calculated with either the thermodynamic or the virial estimator must be the same for all N. In Appendix B, to underscore the importance of the β derivative term in Eq. (3.4), we calculate the internal energy for a semiclassical approximation to the harmonic oscillator density matrix.

C. Hamiltonian estimator

The previous two estimators are both derived from thermodynamic considerations, but we can also calculate the average energy by a direct application of the Hamiltonian to the density operator. As mentioned earlier, because the kinetic energy operator is not diagonal in the position representation, the symmetry of the Trotter factorization [Eq. (2.9)] is important when we directly apply the operator to Eq. (2.11). Since the Hamiltonian estimator does not involve any temperature derivatives, however, generalizing it to temperature-dependent potentials is trivial. The Hamiltonian estimator is

$$E_h=\langle T\rangle+\langle\overline{V}\rangle, \tag{3.6}$$

where [37]

$$\langle T\rangle=\left\langle\frac{N}{2\beta}-\frac{mN}{2\hbar^2\beta^2}\sum_{i=1}^{N}(x_i-x_{i+1})^2-\frac{1}{N}\sum_{i=1}^{N}\left[\frac{1}{2}(x_i-x_{i+1})\frac{\partial}{\partial x_i}\overline{V}(x_i,\beta/N)+\frac{\hbar^2\beta}{4mN}\frac{\partial^2}{\partial x_i^2}\overline{V}(x_i,\beta/N)-\frac{\hbar^2\beta^2}{8mN^2}\left(\frac{\partial\overline{V}(x_i,\beta/N)}{\partial x_i}\right)^2\right]\right\rangle, \tag{3.7}$$

$$\langle\overline{V}\rangle=\left\langle\frac{1}{N}\sum_{i=1}^{N}\overline{V}(x_i,\beta/N)\right\rangle. \tag{3.8}$$

Sustitution of the Tsallis effective potential gives

$$E_h = \left\langle \frac{N}{2\beta} - \frac{mN}{2\hbar^2\beta^2}\sum_{i=1}^{N}(x_i - x_{i+1})^2 + \frac{1}{\beta}\sum_{i=1}^{N}\ln\left\{1 + \frac{\beta}{N}V(x_i)\right\} - \frac{1}{N}\sum_{i=1}^{N}\left[\frac{1}{2}\frac{(x_i - x_{i+1})\frac{\partial}{\partial x_i}V(x_i)}{\left\{1+\frac{\beta}{N}V(x_i)\right\}} + \frac{\hbar^2\beta}{4mN}\frac{\frac{\partial^2}{\partial x_i^2}V(x_i)}{\left\{1+\frac{\beta}{N}V(x_i)\right\}} - \frac{3\hbar^2\beta^2}{8mN^2}\left(\frac{\frac{\partial}{\partial x_i}V(x_i)}{1+\frac{\beta}{N}V(x_i)}\right)^2\right]\right\rangle. \tag{3.9}$$

This estimator is seldom used in path integral simulations on account of the spatial derivatives of the potential which must be computed [37]. In general, the Hamiltonian estimator will converge with N to the exact energy differently than two previous estimators, even in the primitive approximation to the path integral. In particular, E_h converges from above, while E_t and E_v converge from below [38]. This property has been used previously to judge the convergence of the energy with respect to N [39].

IV. METHODS

In this paper, path integrals are evaluated using two different numerical schemes. For the simple one-dimensional systems we are working with, it proves convenient to make use of an established technique, based on numerical quadratures. We use this method to evaluate and compare results based on Eqs. (2.12) and (2.15). The technique is described below.

To address the problem of broken ergodicity in path integral simulations, we develop a path integral Monte Carlo (PIMC) technique. We describe our Monte Carlo method, based on generalized parallel sampling [40], below.

A. Numerical matrix multiplication

Numerical matrix multiplication (NMM) [41,42] is an accurate and efficient way of evaluating density matrices for low-dimensional systems [43]. The technique is not well suited for many-dimensional systems, but for the one-dimensional systems studied here, it is completely equivalent to and much more efficient than Monte Carlo methods.

NMM is based on the observation that

$$\rho(x_1,x_2;\beta) = \int dx_3 \rho(x_1,x_3;\beta/2)\rho(x_3,x_2;\beta/2). \tag{4.1}$$

When the density matrix is discretized and stored as a matrix, one can find the density matrix at $\beta/2$ by repeated iterations of Eq. (4.1),

$$\rho(x_1,x_3;\beta/2) = \int dx_4 \rho(x_1,x_4;\beta/4)\rho(x_4,x_3;\beta/4),$$

$$\vdots \tag{4.2}$$

$$\rho(x_1,x_{n+1};\beta/2^{n-1}) = \int dx_{n+2}\rho^{(0)}(x_1,x_{n+2};\beta/2^n)\rho^{(0)}(x_{n+2},x_{n+1};\beta/2^n). \tag{4.3}$$

The subscripts on the dummy integration variables are simply indicated for consistency, with n being the number of iterations. The hierarchy is closed by Eqs. (2.13) and (2.14) with $2^n = N$.

Thirumalai, Bruskin, and Berne [42] give a useful prescription for these calculations, which we follow. A grid for our integrations is initially set up with $2M+1$ points in each direction, running from $-S/2$ to $S/2$ and with spacing Δ. This implies $S = M\Delta$. Writing out the numerical integration rule gives

$$\rho(i\Delta,j\Delta;\beta) = \Delta\sum_{k=-M}^{M}\rho(i\Delta,k\Delta;\beta/2)\rho(k\Delta,j\Delta;\beta/2). \tag{4.4}$$

We need to choose two of S, Δ, and M, such that we reach convergence. In the calculations presented here, we started by setting

$$S = 8\left[\frac{\hbar}{2m\omega}\coth(\beta\hbar/2N)\right]^{1/2}, \tag{4.5}$$

TABLE I. Summary of NMM grid discretization parameters at different temperatures.

N	2α [a]	2α [b]
2	10^{-5}	10^{-3}
4	10^{-4}	10^{-2}
8	10^{-4}	10^{-2}
16	10^{-4}	5×10^{-2}
32	10^{-3}	10^{-1}
64	10^{-3}	5×10^{-1}
128	10^{-2}	7.5×10^{-1}
256	10^{-1}	
512	10^{-1}	
1024	3×10^{-1}	
2048	7.5×10^{-1}	

[a]Low temperature, e.g., harmonic oscillator with $m=1$ and $\hbar\omega\beta=20$.

[b]High temperature, e.g., harmonic oscillator with $m=1$ and $\hbar\omega\beta=1$.

which is eight standard deviations from the average position for a quantum harmonic oscillator of mass m at the highest temperature. A grid spacing Δ was determined, keeping in mind the breadth of the Gaussian in Eq. (2.14)

$$\rho_0(i\Delta,j\Delta;\beta/N)=\sqrt{\frac{mN}{2\pi\hbar^2\beta}}\exp[-\alpha(i-j)^2], \quad (4.6)$$

where

$$\alpha=\frac{-mN\Delta^2}{2\hbar^2\beta}. \quad (4.7)$$

We choose Δ small enough that the free particle density matrix is sampled well in the space of i and j. That is, α should be small. Rewriting Eq. (4.7), we have

$$\Delta=\hbar\sqrt{2\alpha\beta/mN}. \quad (4.8)$$

We set Δ implicitly by choosing α in Eq. (4.8). All other parameters on the right hand side are determined by the system.

Ordinarily, one begins a calculation by choosing n so that the high temperature approximation in Eq. (2.13) is valid. Since we are addressing the quality of this approximation, as it depends upon the treatment of the potential energy, we start by assigning S and α instead. Table I summarizes the values of α used in our NMM calculations. We chose α both to expedite our computations and to have a quantitative agreement (in the primitive approximation) with the analytic finite-N harmonic oscillator averages [17,44].

Adapting the energy estimators of the preceding section to NMM, we calculated the thermodynamic estimator using a three-point approximation to the derivative

$$E_t=-\frac{\partial}{\partial\beta}\ln Z\approx\frac{-\ln Z(\beta+\delta)+\ln Z(\beta-\delta)}{2\delta}+O(\delta^2), \quad (4.9)$$

where $\delta=10^{-4}$. The Hamiltonian estimator was calculated with formula (3.6), and

$$\langle\overline{V}\rangle=\frac{1}{Z}\int dx\,\overline{V}(x,\beta)\rho(x,x), \quad (4.10)$$

$$\langle T\rangle=\frac{\langle p^2\rangle}{2m}=-\frac{1}{Z}\frac{\hbar^2}{2m}\int dx\,\frac{\partial^2}{\partial x^2}\rho(x,y)\bigg|_{y=x}. \quad (4.11)$$

In the last integral above, the second derivative was taken along one of the dimensions of the density matrix before setting $y=x$. We performed this differentiation numerically using a five-point approximation for the second derivative. To ensure that the numerical error in the derivative was small, the second derivative was also taken by successive iterations of a five-point approximation to the first derivative. The difference between these two approximations to the second derivative was kept small.

The virial estimate of the energy was calculated using the obvious quadrature (see Appendix B).

B. Generalized parallel sampling

Along with a direct comparison of the rates of convergence in N, based on Eqs. (2.12) and (2.15), we also investigate application of the Tsallis effective potential as part of a proposed Monte Carlo method for enhanced sampling. In classical simulations where broken ergodicity is present, Straub and Andricioaei have developed methods for calculating Maxwell-Boltzmann averages using Tsallis statistical distributions [23]. One of their methods is umbrella sampling [45], which is generally not efficient when there is insufficient overlap between the sampling distribution and the physical one (at $q=1$, for example). Parallel tempering [46–50] is an alternative method in which several Monte Carlo simulations are performed simultaneously at different temperatures. With a given probability, pairs of configurations at different temperatures may be exchanged. Such exchanges are accepted with probability

$$p=\min\left[1,\frac{p_{T_2}(\mathbf{x}_1)p_{T_1}(\mathbf{x}_2)}{p_{T_1}(\mathbf{x}_1)p_{T_2}(\mathbf{x}_2)}\right], \quad (4.12)$$

where $p_{T_i}(\mathbf{x}_j)$ is the probability of configuration j at temperature T_i. The composite Markov chain of all random walks, including the exchanges, is itself a Markov process [48].

Just as the sampling distribution need not be related to the natural distribution in the umbrella sampling method, we can also generalize the parallel tempering method. Instead of a series of distributions at different temperatures, the method may be generalized by incorporating a number of simultaneous Monte Carlo simulations, each of which may sample a different probability distribution. In the present context, we generate these distributions using a family of effective po-

tentials, each parametrized by a different value of q in Eq. (2.4). Equation (4.12) becomes

$$p=\min\left[1,\frac{p_{q_2}(\mathbf{x}_1)p_{q_1}(\mathbf{x}_2)}{p_{q_1}(\mathbf{x}_1)p_{q_2}(\mathbf{x}_2)}\right], \tag{4.13}$$

where, in our path integral case,

$$p_q(\mathbf{x})\propto\exp[-\bar{\Phi}(\mathbf{x})]. \tag{4.14}$$

The same technical concerns that one has with the standard parallel tempering method carry over to this generalization, which we call generalized parallel sampling (GPS) [40]. These concerns include ensuring that there is sufficient overlap among the various distributions that exchanges are frequently accepted. Furthermore, at least one of the simulations (say at the highest q value) should quickly converge to its equilibrium distribution. That is, the largest q should be chosen such that there is no broken ergodicity associated with sampling $p_q(\mathbf{x})$.

In our simulations we ran PIMC in parallel on k systems, each with q set according to

$$q_j=\frac{\epsilon}{\gamma(\eta-\epsilon)}\left[\left(\frac{\eta}{\epsilon}\right)^{(j-1)/(k-1)}-1\right]+1, \tag{4.15}$$

where, $1<j<k$. For $\eta\approx\epsilon$, the q_j's are approximately linearly related. For the GPS calculations, we did not require that $q=1+1/N$. Instead, for the highest q we have $q_k=1+1/\gamma$, from Eq. (4.15). When exchanges are not attempted, each distribution (4.14) was sampled using the standard PIMC.

Choosing the qs according to Eq. (4.15) allows for close spacing between low values of q, which can mitigate any correlation between the distributions at q_1 and q_k. Although we have not found it necessary here, it is also possible to choose the set of qs in a more systematic way, based on the acceptance ratio for exchange moves [40].

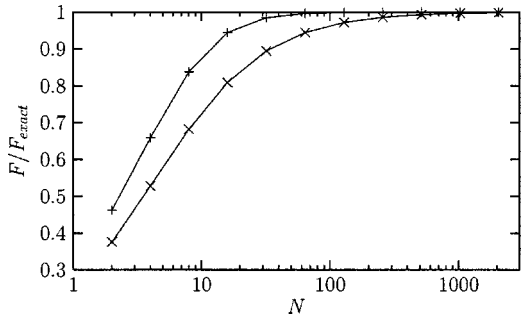

FIG. 1. Estimates of the Helmholtz free energy of the quantum mechanical harmonic oscillator. N is the number of ''beads'' in the path integral. We have $m=1$ and $\hbar\omega\beta=20$. Both the standard primitive approximation (+) and use of the Tsallis effective potential (×) are shown.

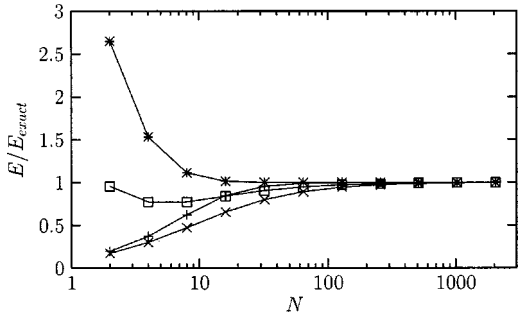

FIG. 2. Internal energy estimates for the quantum mechanical harmonic oscillator. N is the number of ''beads'' in the path integral. We have $m=1$ and $\hbar\omega\beta=20$. Shown are the data from the standard primitive approximation using the Hamiltonian estimator (*) or the thermodynamic estimator (+) and from use of the Tsallis effective potential with the Hamiltonian estimator (□) or the thermodynamic estimator (×).

V. RESULTS AND DISCUSSION

We first applied the effective potential substitution to the one-dimensional harmonic oscillator. NMM calculations were performed to determine the convergence behavior, with N, of path integral averages. We compared these results with those calculated using the primitive approximation. We repeated these NMM calculations for a bistable one-dimensional potential.

In addition, for the bistable potential, we applied the GPS method described in the preceding section. The GPS results were compared with calculations done using standard PIMC methods.

A. Harmonic oscillator

For the harmonic oscillator

$$V(x)=\frac{1}{2}m\omega^2x^2, \tag{5.1}$$

we have calculated the free energy, $F=\beta^{-1}\ln Z$, along with the internal energy (using the three estimators described above) and the standard deviation of the position operator. For the harmonic oscillator, all of these observables can be

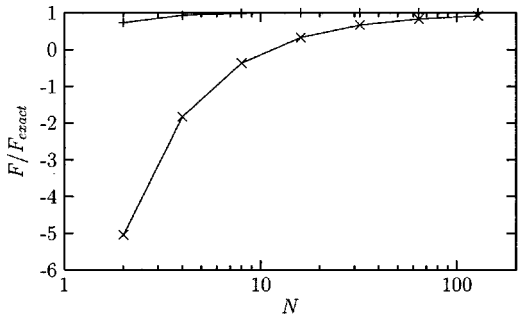

FIG. 3. Estimates of the Helmholtz free energy of the quantum mechanical harmonic oscillator. N is the number of ''beads'' in the path integral. We have $m=1$ and $\hbar\omega\beta=1$. Both the standard primitive approximation (+) and use of the Tsallis effective potential (×) are shown.

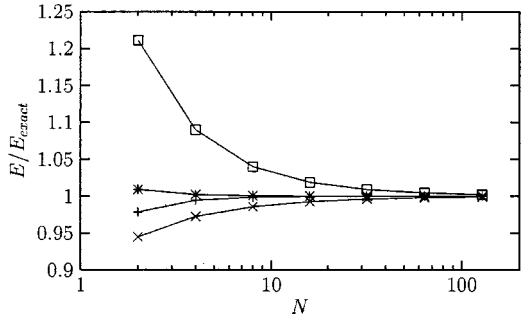

FIG. 4. Internal energy estimates for the quantum mechanical harmonic oscillator. N is the number of ''beads'' in the path integral. We have $m=1$ and $\hbar\omega\beta=1$. Shown are the data from the standard primitive approximation using the Hamiltonian estimator (*) or the thermodynamic estimator (+) and from use of the Tsallis effective potential with the Hamiltonian estimator (□) or the thermodynamic estimator (×).

worked out analytically for any N [17,44,38]. We reproduced the analytical results using NMM and then repeated the calculations using the effective action [Eq. (2.15)].

We looked at the harmonic oscillator at a low temperature ($\hbar\omega\beta=20$), where the number of beads required to get good approximations for the observables was relatively high, and also at a higher temperature ($\hbar\omega\beta=1$). Our results are summarized in Figs. 1–4. Since the thermodynamic and virial estimators give the same averages by construction, differences between the two estimates of the internal energy in simulations are due to the statistical issues not present in NMM. These two estimators are, therefore, equal to one another in NMM calculations. Differences in E_t and E_h, instead, give an indication of the sufficiency of N [38], and disappear as $N\to\infty$. The free energy, by contrast, does not depend on selecting an estimator and gives a direct measure of the convergence of the path integral approximation to the partition function.

As expected, Figs. 1 and 2 show that the free energy and the internal energy converge to the exact result for large N when we use the Tsallis effective potential. We also note that

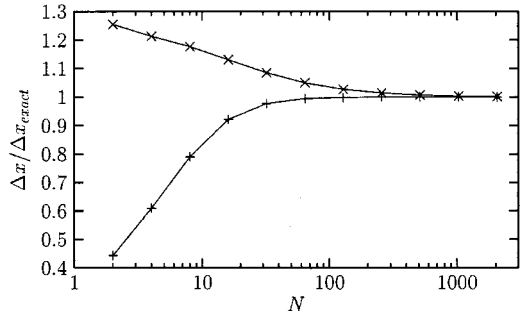

FIG. 5. Root-mean-squared deviation of the distribution in position. N is the number of ''beads'' in the path integral. We have $m=1$ and $\hbar\omega\beta=20$. Both the standard primitive approximation (+) and use of the Tsallis effective potential (×) are shown.

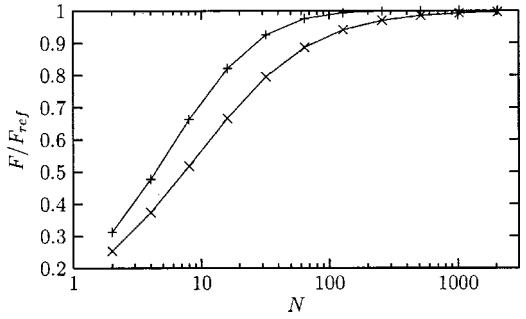

FIG. 6. Estimates for the Helmholtz free energy of a quantum mechanical bistable potential. N is the number of ''beads'' in the path integral. We have $a=1$, $m=1$, $\hbar=1$, $\omega^2=8\hbar/ma^2$, and $\beta=20$. Both the standard primitive approximation (+) and use of the Tsallis effective potential (×) are shown.

the convergence is relatively poor in comparison with the standard primitive approximation. Figures 3 and 4 show that the relative convergence due to the application of the effective potential does not improve at higher temperatures.

Having computed $\Delta x=\sqrt{\langle x^2\rangle-\langle x\rangle^2}$ we can draw a comparison between the standard and effective potential approaches. In Fig. 5, we see that while the width of the distribution in the standard approximation decreases for small N, the opposite behavior is observed for the path integral using the effective action. Note, however, that since we have $q=1+1/N$ in these calculations, q increases with decreasing N.

The decrease of Δx for small N in the primitive approximation, along with that of the free energy and the thermodynamic estimate for the internal energy, is well known [17,2] and has been described as ''classical collapse'' [44], since the configurational distribution tends toward the classical one. Using the effective action appears to mitigate this collapse, at least for Δx. In any case, the fact that the quantum mechanical configurational distribution becomes broadened with increasing q suggests that the effective potential may prove useful as part of an enhanced sampling scheme in systems with high barriers.

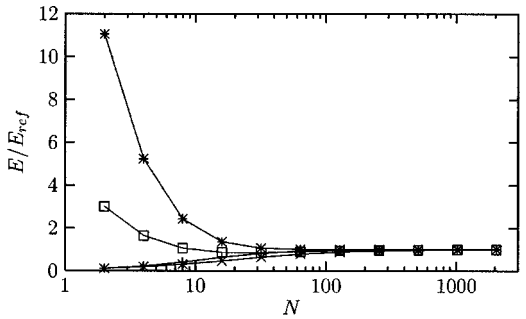

FIG. 7. Internal energy estimates for a quantum mechanical bistable potential. N is the number of ''beads'' in the path integral. We have $a=1$, $m=1$, $\hbar=1$, $\omega^2=8\hbar,ma^2$, and $\beta=20$. Shown are the data from the standard primitive approximation using the Hamiltonian estimator (*) or the thermodynamic estimator (+) and from use of the Tsallis effective potential with the Hamiltonian estimator (□) or the thermodynamic estimator (×).

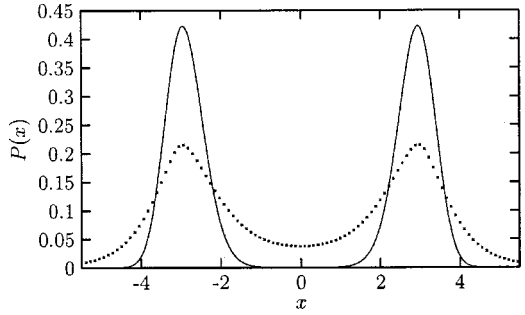

FIG. 8. Probability distribution for the quantum mechanical double well. The solid curve is for $q=1$ and the dotted curve for $q=2$. We have $N=8$, $a=3$, $m=1$, $\hbar=1$, $\omega^2=40\hbar/ma^2$, and $\beta=4$.

B. Quartic bistable potential

We have investigated a bistable potential

$$V=\frac{1}{8}\frac{m\omega^2}{a^2}(x-a)^2(x+a)^2. \tag{5.2}$$

First, using the same approach as with the harmonic oscillator, we compared the convergence of thermodynamic averages between the standard primitive approximation and use of the effective potential. The results are summarized in Figs. 6 and 7. Again, observables converge faster in N when calculated using the standard primitive approximation. The reference energies in these figures (e.g. F_{ref}) come from the fully converged NMM calculations, and are essentially exact.

Next, we applied the GPS technique to the system and compared with the standard PIMC method. In these calculations, we did not maintain $q=1+1/N$ in the effective potential, but rather set the various qs according to Eq. (4.15). The parameters of the simulation were adjusted such that broken ergodicity would be present. Looking at Fig. 8, we note that

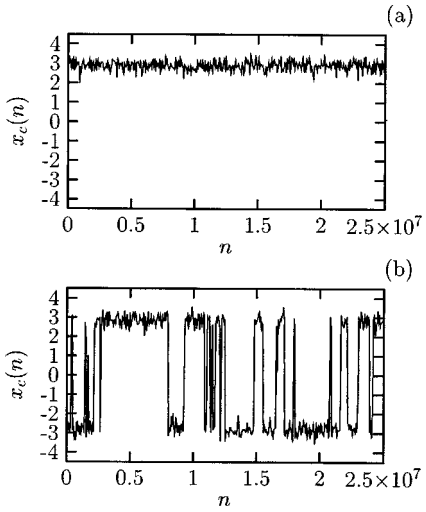

FIG. 9. Position of the path integral centroid x_c, as a function of number of Monte Carlo moves n. The number of Monte Carlo moves is the total number, summed over all particles in all polymer walkers in each simulation. The GPS centroid is for the walker at $q=1$. Simulations are (a) PIMC and (b) GPS.

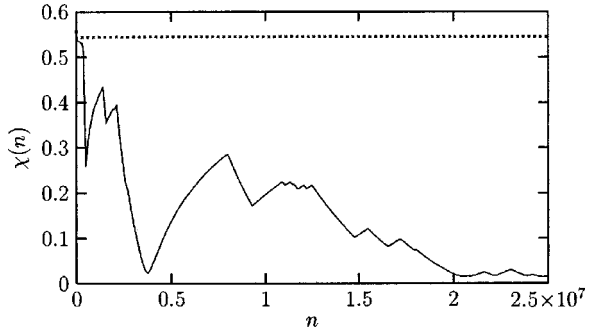

FIG. 10. χ as a function of number of Monte Carlo moves n. The number of Monte Carlo moves is the total number, summed over all particles in all polymer walkers in each simulation. The GPS χ is calculated for the walker at $q=1$. The solid line is a typical GPS run and the dotted line is a standard PIMC simulation.

the configurational distribution at $q=1$ (physical potential), in contrast to the distribution at $q=2$ (effective potential), has little probability of being in the barrier region. This is precisely the type of situation in which a parallel sampling method is useful.

Based on NMM calculations, it was determined that $N=8$ was adequate for simulation of this system in the primitive approximation. In the GPS calculation therefore, each of the parallel walkers was a polymer ring with eight beads. There were $k=5$ different qs, set according to Eq. (4.15) with $\epsilon=10^{-3}$, $\gamma=1$ and $\eta=1000$. Exchanges were made among the five walkers, between rings of neighboring q. Such exchanges were attempted with probability 0.025. When an exchange was attempted, walkers not involved in the exchange were updated with standard PIMC moves. When no exchange was attempted, all walkers attempted PIMC moves.

As a measure of convergence, we have calculated χ, where [7]

$$\chi^2(n)=\int dx\left[\frac{\rho(x,x;n)}{Z(n)}-\frac{\rho_{exact}(x,x)}{Z_{exact}}\right]^2, \tag{5.3}$$

and $\rho(x,x;n)/Z(n)$ is the normalized spatial probability distribution after n Monte Carlo moves.

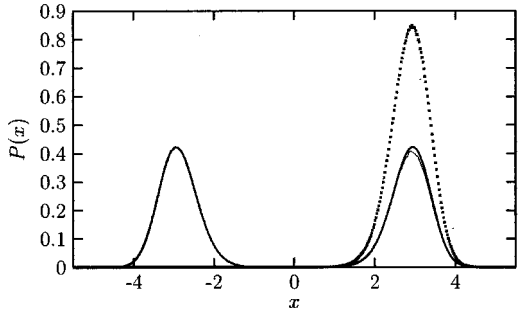

FIG. 11. Probability distribution for the double well potential. The thick solid is the ''exact'' result, calculated from NMM. The thin solid curve is the GPS disribution and the dotted curve is the standard PIMC result. We have $N=8$, $a=3$, $m=1$, $\hbar=1$, $\omega^2=40\hbar/ma^2$, and $\beta=4$.

TABLE II. Summary of PIMC and GPS results for the quartic bistable potential.

	NMM	PIMC	GPS
$\overline{\chi}$		5.452×10^{-1}	7.699×10^{-2}
$\sigma^2(\chi)$		1.580×10^{-8}	2.048×10^{-3}
$\overline{\Delta x}$	2.924	4.799×10^{-1}	2.880
$\sigma^2(\Delta x)$		3.026×10^{-8}	2.063×10^{-3}

In Fig. 9, we see that the center of mass (centroid) of the $q=1$ walker in our GPS simulation crosses the barrier frequently compared with that of the standard PIMC simulation, which is completely trapped in one of the wells. All plots related to the Monte Carlo simulations are normalized for computer time. That is, the number of Monte Carlo moves is the same for the single chain in the standard PIMC simulation as the total number over all chains in the GPS simulation.

From Fig. 10 we see that the GPS distribution is converging to the exact one. From the standard PIMC simulation, $\chi(n)$ is not converging. The distributions after representative GPS and standard PIMC simulations are shown in Fig. 11. Each simulation involved a total of 4×10^7 Monte Carlo moves.

Data averaged over ten independent simulations are presented in Table II. Relative to the standard PIMC approach, the GPS simulations converged to a significantly smaller average χ, and were able to predict the root-mean-square deviation of the configurational distribution with a reasonable accuracy. In all of the PIMC simulations, the isomorphic polymer chain remained trapped on one side of the barrier.

VI. CONCLUSIONS

We have shown that direct substitution of the Tsallis effective potential into the path integral does not generally enhance convergence. In the simple one-dimensional systems investigated here, neither the free energy nor the internal energy converged more rapidly in N after making the substitution. We did note however, that the configurational distributions of quantum systems undergo broadening similar to that observed in classical systems [34,28,23,24], as q is increased from unity. This broadening has been used as the basis for a generalized parallel sampling technique for path integrals.

For a simple quantum system where broken ergodicity prohibits convergence of standard PIMC methods, we have successfully applied a Monte Carlo method for enhanced sampling, GPS, to path integrals. This method dramatically enhances the frequency of barrier crossing for the isomorphic polymer chain. It does not, however, mitigate the problem of stiff bonds as N becomes large. For simulations requiring large N, and where broken ergodicity is present, the GPS technique can readily be combined with the existing path integral methods for stiff bonds—normal mode techniques, for example.

Although GPS allows for accurate sampling of the quantum configurational distribution in systems with broken ergodicity, the underlying reason for its success—that broken ergodicity is not present at high q—suggests that other enhanced sampling schemes involving the Tsallis effective potential could also be usefully adapted to path integral simulations. For example, the ''q-jumping'' method of Andricioaei and Straub [34], which is a special case of GPS [40]. It would be interesting to compare the numerical efficiency of such alternative approaches with that of GPS.

For path integral simulations involving the Tsallis effective potential, in the form given by Eqs. (2.3), (2.4), and (2.15), we have introduced three estimators for the internal energy. In path integral simulations that make use of the Tsallis effective potential, agreement between E_h and E_t (or E_v) can be useful to judge the sufficiency of N, just as is the case in the primitive approximation. Indeed, the same criterion is broadly applicable and can be extended, using estimators presented here, to any path integral simulation involving a temperature-dependent effective potential.

ACKNOWLEDGMENTS

J.E.S. acknowledges the generous support of the National Science Foundation (Grant No. CHE-9975494).

APPENDIX A

Below, we follow Herman, Bruskin, and Berne's derivation of the virial estimator [35]. We start by rewriting Eq. (3.2)

$$E_t=\left\langle \frac{N}{2\beta}-\alpha_N+\lambda_N+\delta_N \right\rangle, \tag{A1}$$

where

$$\alpha_N=\frac{Nm}{2\hbar^2\beta^2}\sum_{i=1}^{N}(x_i-x_{i+1})^2, \tag{A2}$$

$$\lambda_N=\frac{1}{N}\sum_{i=1}^{N}\overline{V}(x_i,\beta), \tag{A3}$$

$$\delta_N=\frac{1}{N}\sum_{i=1}^{N}\beta\frac{\partial}{\partial\beta}\overline{V}(x_i,\beta). \tag{A4}$$

Next, consider the following average:

$$\left\langle \sum_{i=1}^{N} x_i\frac{\partial U_N}{\partial x_i}\right\rangle=\frac{\int dx_1\cdots dx_N\left[\sum_{i=1}^{N} x_i\frac{\partial U_N}{\partial x_i}\right]e^{-\beta U_N}}{\int dx_1\cdots dx_N e^{-\beta U_N}}, \tag{A5}$$

where

$$U_N=\alpha_N+\lambda_N. \tag{A6}$$

Since

$$e^{-\beta U_N} x_i \frac{\partial U_N}{\partial x_i} = -\frac{1}{\beta} x_i \frac{\partial e^{-\beta U_N}}{\partial x_i}, \tag{A7}$$

an integration by parts gives

$$\left\langle \sum_{i=1}^{N} x_i \frac{\partial U_N}{\partial x_i} \right\rangle = \frac{1}{\beta} \sum_{i=1}^{N} \left\langle \frac{\partial x_i}{\partial x_i} \right\rangle = \frac{N}{\beta}, \tag{A8}$$

or

$$\left\langle \sum_{i=1}^{N} x_i \frac{\partial \alpha_N}{\partial x_i} \right\rangle + \left\langle \sum_{i=1}^{N} x_i \frac{\partial \lambda_N}{\partial x_i} \right\rangle = \frac{N}{\beta}. \tag{A9}$$

Since α_N is a homogeneous function of degree 2 of all the x_i, Euler's theorem can be invoked,

$$\sum_{i=1}^{N} x_i \frac{\partial \alpha_N}{\partial x_i} = 2\alpha_N. \tag{A10}$$

Equation (A9) can be recast as

$$\left\langle \frac{N}{2\beta} - \alpha_N \right\rangle = \left\langle \frac{1}{2N} \sum_{i=1}^{N} x_i \frac{\partial \overline{V}(x_i,\beta)}{\partial x_i} \right\rangle. \tag{A11}$$

Substitution back into Eq. (A1) yields Eq. (3.4).

APPENDIX B

To emphasize the necessity of including the β-derivative term in Eq. (3.4), we examine an application of the generalized virial estimator to a semiclassical approximation for the harmonic oscillator distribution function. To begin, consider the following effective potential:

$$\overline{V}(x,\beta) = \frac{1}{2} m\omega^2 x^2 + \frac{\beta(\hbar\omega)^2}{24} \tag{B1}$$

from a variational approach of Feynman [51,52].

We verify that the internal energy calculated using our virial estimator, Eq. (3.4), agrees with that calculated directly from the partition function (i.e., E_t). We begin by writing our estimator in a form appropriate for averaging over the density matrix

$$E_v = \frac{1}{Z} \int dx \left[\overline{V}(x,\beta) + \beta \frac{\partial}{\partial \beta} \overline{V}(x,\beta) + \frac{1}{2} x \frac{\partial \overline{V}(x,\beta)}{\partial x} \right] \rho(x,x), \tag{B2}$$

$$\equiv I_1 + I_2 + I_3, \tag{B3}$$

The density matrix appearing above will be

$$\rho(x,x) = \left(\frac{m}{2\pi\hbar^2\beta} \right)^{1/2} \exp[-\beta \overline{V}(x,\beta)] \tag{B4}$$

in the semiclassical analysis that we consider here. In our NMM calculations, however, $\rho(x,x)$ is determined numerically and will converge to the exact diagonal of the density matrix after sufficiently many iterations. In that case, Eq. (B3) will give the exact quantum internal energy.

But considering now the semiclassical approximation to the diagonal, the partition function is

$$Z = \int dx \rho(x,x) = \frac{e^{-(\beta\hbar\omega)^2/24}}{\beta\hbar\omega}, \tag{B5}$$

which helps us to write

$$I_1 = \frac{1}{2\beta} + \frac{\beta(\hbar\omega)^2}{24}, \tag{B6}$$

$$I_2 = \frac{\beta(\hbar\omega)^2}{24}, \tag{B7}$$

$$I_3 = \frac{1}{2\beta}, \tag{B8}$$

and finally

$$E_v = \frac{1}{\beta} + \frac{\beta(\hbar\omega)^2}{12}. \tag{B9}$$

Instead, from the partition function,

$$E_t = -\frac{\partial}{\partial \beta} \ln Z = \frac{1}{\beta} + \frac{\beta(\hbar\omega)^2}{12}. \tag{B10}$$

Equation (B5) leads to a well-known semiclassical estimate for the free energy of the quantum mechanical harmonic oscillator [51,52]. For the virial estimator to give the corresponding internal energy, the term involving the β derivative I_2 must be included.

[1] D. Chandler and P. G. Wolynes, J. Chem. Phys. **74**, 4078 (1981).
[2] M. P. Allen and D. J. Tildesley, *Computer Simulation of Liquids* (Oxford University Press, Oxford, 1987).
[3] B. J. Berne and D. Thirumalai, Annu. Rev. Phys. Chem. **37**, 401 (1986).
[4] R. G. Palmer, Adv. Phys. **31**, 669 (1982).
[5] D. Thirumalai, R. D. Mountain, and T. R. Kirkpatrick, Phys.

Rev. A **39**, 3563 (1989).
[6] R. D. Mountain and D. Thirumalai, Physica A **210**, 453 (1994).
[7] J. Cao and B. J. Berne, J. Chem. Phys. **92**, 1980 (1990).
[8] R. D. Coalson, J. Chem. Phys. **85**, 926 (1986).
[9] J. D. Doll and D. L. Freeman, J. Chem. Phys. **80**, 2239 (1984).
[10] D. L. Freeman and J. D. Doll, J. Chem. Phys. **80**, 5709 (1984).
[11] M. Eleftheriou, J. D. Doll, E. Curotto, and D. L. Freeman, J. Chem. Phys. **110**, 6657 (1999).
[12] M. Sprik, M. L. Klein, and D. Chandler, Phys. Rev. B **31**, 4234 (1985).
[13] H. De Raedt and B. De Raedt, Phys. Rev. A **28**, 3575 (1983).
[14] M. Suzuki, J. Stat. Phys. **43**, 883 (1986).
[15] M. Suzuki, Commun. Math. Phys. **163**, 491 (1994).
[16] D. Thirumalai and B. J. Berne, J. Chem. Phys. **79**, 5029 (1983).
[17] K. S. Schweizer, R. M. Stratt, D. Chandler, and P. G. Wolynes, J. Chem. Phys. **75**, 1347 (1981).
[18] R. A. Friesner and R. M. Levy, J. Chem. Phys. **80**, 4488 (1984).
[19] C. H. Mak and H. C. Andersen, J. Chem. Phys. **92**, 2953 (1990).
[20] J. Cao and B. J. Berne, J. Chem. Phys. **92**, 7531 (1990).
[21] M. Messina, B. C. Garrett, and G. K. Schenter, J. Chem. Phys. **100**, 6570 (1994).
[22] C. E. Chao and H. C. Andersen, J. Chem. Phys. **107**, 10 121 (1997).
[23] J. E. Straub and I. Andricioaei, Braz. J. Phys. **29**, 179 (1999).
[24] I. Andricioaei and J. E. Straub, in *Nonextensive Statistical Mechanics and Its Applications*, edited by S. Abe and Y. Okamoto, Lecture Notes in Physics Vol. 560 (Springer-Verlag, Berlin, 2001), Chap. IV.
[25] C. Tsallis, J. Stat. Phys. **52**, 479 (1988).
[26] L. S. Schulman, *Techniques and Applications of Path Integration* (Wiley, New York, 1981).
[27] A. K. Rajagopal and C. Tsallis, Phys. Lett. A **257**, 283 (1999).
[28] J. E. Straub and I. Andricioaei, in *Proceedings of the Second International Symposium on Algorithms for Macromolecular Modelling, Berlin, 1997*, edited by P. Deuflhard *et al.*, Lecture Notes in Computational Science and Engineering Vol. 4 (Springer-Verlag, Berlin, 1998), Chap. 11.
[29] C. Tsallis, R. S. Mendes, and A. R. Plastino, Physica A **261**, 534 (1998).
[30] In particular, there exists a normalized version of the second constraint [29], leading to a different equilibrium distribution from Eq. (2.5), and hence a different effective potential from Eq. (2.4). For our purposes, however, the effective potential corresponding to the normalized constraint has a disadvantage over the present choice; it must be defined in terms of a ''renormalized'' temperature involving integrals over the configurational distribution. This renormalized temperature obscures the formal connection between the nonextensive thermostatistics and the thermal density matrix [23,24], and makes the subsequent computations less tractable.
[31] B. M. Boghosian, Braz. J. Phys. **29**, 91 (1999).
[32] I. Andricioaei and J. E. Straub, Phys. Rev. E **33**, 3055 (1996).
[33] I. Andricioaei and J. E. Straub, Physica A **247**, 553 (1997).
[34] I. Andricioaei and J. E. Straub, J. Chem. Phys. **107**, 9117 (1997).
[35] H. F. Herman, E. J. Bruskin, and B. J. Berne, J. Chem. Phys. **76**, 5150 (1982).
[36] A. Giansanti and G. Jacucci, J. Chem. Phys. **89**, 7454 (1988).
[37] D. M. Ceperley, Rev. Mod. Phys. **67**, 279 (1995).
[38] T. W. Whitfield and J. E. Straub, J. Chem. Phys. **115**, 6834 (2001).
[39] K. J. Runge and G. V. Chester, Phys. Rev. B **38**, 135 (1988).
[40] T. W. Whitfield, L. Bu, and J. E. Straub, Physica A (submitted).
[41] R. G. Storer, J. Math. Phys. **9**, 964 (1968).
[42] D. Thirumalai, E. J. Bruskin, and B. J. Berne, J. Chem. Phys. **79**, 5063 (1983).
[43] E. L. Pollock and D. M. Ceperley, Phys. Rev. B **30**, 2555 (1984).
[44] S. K. Kauffmann and J. Rafelski, Z. Phys. C **24**, 157 (1984).
[45] G. M. Torrie and J. P. Valleau, J. Comput. Phys. **23**, 187 (1977).
[46] E. Marinari and G. Parisi, Europhys. Lett. **19**, 451 (1992).
[47] C. J. Geyer and E. A. Thompson, J. Am. Stat. Assoc. **90**, 909 (1995).
[48] M. C. Tesi, E. J. Janse van Rensburg, E. Orlandini, and S. G. Whittington, J. Stat. Phys. **82**, 155 (1996).
[49] J. P. Neirotti, F. Calvo, D. L. Freeman, and J. D. Doll, J. Chem. Phys. **112**, 10 340 (2000).
[50] F. Calvo, J. P. Neirotti, D. L. Freeman, and J. D. Doll, J. Chem. Phys. **112**, 10 350 (2000).
[51] R. P. Feynman, *Statistical Mechanics: A Set of Lectures* (Addison-Wesley, Reading, MA, 1972).
[52] R. P. Feynman and A. R. Hibbs, *Quantum Mechanics and Path Integrals* (McGraw-Hill, New York, 1965).